https://doi.org/10.5194/acp-2022-407
Preprint. Discussion started: 15 August 2022


Atmospheric Chemistry and Physics Discussions
Open Access

# Nonlinear resonant interactions of atmospheric tides with annual oscillation based on meteor radar observation and reanalysis data

Xiansi Huang[1,2,3] Kaiming Huang[1,2,3] Hao Cheng[1,2] Shaodong Zhang[1,2] Wei Cheng[4]

Chunming Huang[1,2] and Yun Gong[1,2]

[1]School of Electronic Information, Wuhan University, Wuhan, China

[2] Key Laboratory of Geospace Environment and Geodesy, Ministry of Education, Wuhan, China

[3]State Observatory for Atmospheric Remote Sensing, Wuhan, China

[4]Beijing Institute of Applied Meteorology, Beijing, China

Email Address: hkm@whu.edu.cn

Zip code: 430072

https://doi.org/10.5194/acp-2022-407
Preprint. Discussion started: 15 August 2022


Atmospheric Chemistry and Physics Discussions

**Abstract.** Nonlinear interactions among gravity waves and among tides and planetary waves (PWs) have extensively been studied, however, resonant interactions between tides and annual (AO) and semiannual (SAO) oscillations were not reported. By using meteor radar observations and reanalysis data for 9 years, we demonstrate that the sum and difference resonant interactions between the diurnal (DT)/semidiurnal (SDT) tides and the AO/SAO do occur in the mesosphere and lower thermosphere (MLT). Both the frequencies and wavenumbers of the secondary waves in the sum (difference) resonant interactions just equal the sum (difference) frequencies and wavenumbers between the DT/SDT and the AO/SAO. Spectral analysis shows that only the DT, SDT, AO, SAO and their secondary waves are the predominant components in both the zonal and meridional winds at 90 km with the spectral amplitudes of 3.5-17.7 $ms^{-1}$, being much stronger than all the other spectral amplitudes, including the amplitudes (2.1-2.2 $ms^{-1}$) of the relatively strong terdiurnal tide and 16-day PW. At some altitudes in the MLT, the secondary waves are more intense than the DT/SDT, thus in tidal studies, the magnitude of the secondary waves may be regarded as the tidal one if the observational period is not long enough or their spectral peaks are not distinguished carefully.

## 1 Introduction

There are various motions with different temporal and spatial scales in the atmosphere, such as small-scale gravity waves (GWs), large-scale tidal waves and planetary waves (PWs), as well as longer period intraseasonal (ISO), semiannual (SAO) and annual (AO) oscillations. These perturbations play an important role in the circulation and thermal structure of the middle and upper atmosphere due to their ability to transfer energy and momentum among different atmospheric layers and among different latitudinal zones (Andrews et al., 1987). Meanwhile, there are complex coupling and nonlinear interactions among different scale waves and oscillations. For example, GWs and tides modulated by the filtering of PWs or ISOs in the lower atmosphere may drive similar period but out of phase PWs or ISOs in the mesosphere and

https://doi.org/10.5194/acp-2022-407
Preprint. Discussion started: 15 August 2022




lower thermosphere (MLT) as momentum transported by GWs and tides is deposited into the background flow in the MLT due to their dissipation (Eckermann et al., 1997; Jacobi et al., 2006; Cheng et al, 2021). This process is essentially wave-flow coupling through the filtering effect as long as long-period PWs or ISOs are regarded as the temporal varying background field through which short-period GWs and tides propagate. Wave-wave nonlinear interaction is another dynamic process in which new spectral components are excited. In theory, nonlinear interaction comes from the nonlinear advective terms in the dynamic equations. Numerical simulation by Teitelbaum and Vial (1991) clearly showed that two secondary waves with sum and difference frequencies between semidiurnal tide (SDT) and 16-day PW were generated only through nonlinear interactions of SDT and 16-day wave rather than their linear superposition.

Nonlinear resonant interaction in the fluid dynamical context was proposed by Phillips [1960]. For specified wave vectors $\vec{k}$ and frequencies $\omega$, two initial waves with phases $\vec{k}_1 \cdot \vec{r} - \omega_1 t$ and $\vec{k}_2 \cdot \vec{r} - \omega_2 t$ can force a third wave with their sum or difference phase. In other words, if both the wave vector and frequency of a free third mode satisfy the sum or difference matching conditions,

$$\vec{k}_1 \pm \vec{k}_2 = \vec{k}_3 \tag{1}$$

$$\omega_1 \pm \omega_2 = \omega_3 \tag{2}$$

where the subscripts 1, 2 and 3 denote the three interacting waves, resonant interaction occurs and leads to significant energy transfer from the initial waves into the third wave. In the light of the two matching conditions, resonant interactions of small-scale GWs have been extensively investigated (e.g., Yeh and Liu, 1981; Müller et al., 1986; Inhester, 1987; Klostermeyer, 1991; Stenflo, 1998; Yi, 1999; Wüst and Bittner, 2006; Huang et al., 2009; Taklo and Choi, 2020), even in a sheared, dissipative and rotating atmosphere (Fritts et al., 1992; Vanneste, 1995; Axelsson et al., 1996; Huang et al., 2014; Achatz et al., 2017; Chatterjee and Misra, 2021; Voelker et al, 2021), and in the uniform and nonuniform plasmas (Stenflo, 1994; Stenflo and Shukla, 2009). For large-scale tides and PWs, many scientists studied their resonant interactions based

https://doi.org/10.5194/acp-2022-407
Preprint. Discussion started: 15 August 2022


Atmospheric Chemistry and Physics Discussions
Open Access
EGU

on general circulation models (GCMs) and ground-based and satellite-borne observations by using the matching condition ($n_1 \pm n_2 = n_3$) of zonal wavenumbers $n$ instead of the wave vector matching condition (Kamalabadi et al., 1997; Jacobi et al., 1998, 2001; Pancheva et al., 2000, 2002; Pancheva and Mitchell, 2004; Liu et al., 2007; Palo et al., 2007; Kumar et al., 2008; McCormack et al., 2010; Babu et al., 2011; Chang et al., 2011a, 2011b; Yue et al., 2012; Huang et al., 2013a, 2013b; He and Chau, 2019).

Although nonlinear interactions between atmospheric waves have attracted wide attention, interactions of both global-scale tides and annual and semiannual oscillations were not reported yet. As we know, tides have a wave structure, but AO and SAO do not, thus it remains unclear whether they can interact with each other in the realistic atmosphere. Atmospheric tides are the persistent global perturbations and are generated mainly by radiation heating from the Sun (Lindzen and Chapman, 1969; Forbes and Garrett, 1979), in consequence, diurnal tide (DT) has a period of a solar day, and a westward wavenumber $n$= -1 due to the westward migration of the Sun in the sky from the view of the Earth. Besides DT, there are its high-order harmonics in the atmosphere, among which SDT with a period of 12 h and a wavenumber of $n$= -2 is the strongest component (Chapman and Lindzen, 1970; Hagan et al., 1999). Atmospheric AO and SAO are slow periodic changes of the zonal and meridional winds and temperature without phase propagation in the zonal direction. The periods of AO and SAO are 2-3 orders of magnitude larger than those of tides, thus the identification of sum and difference frequencies between tides and AO/SAO from tides is limited due to the requirement of rather long-time observations with high temporal resolution.

In the MLT, atmospheric waves have generally strong amplitudes, thereby, their nonlinear interactions are an important aspect of dynamics in the MLT. In present study, we use the observational and reanalysis data for 9 years to reveal the occurrence of resonant interactions between tides and AO/SAO. In Section 2, the radar observations and reanalysis data are described in brief. In Section 3, nonlinear interactions between DT/SDT and AO/SAO are discussed based on the observational and reanalysis data. A summary is provided

https://doi.org/10.5194/acp-2022-407
Preprint. Discussion started: 15 August 2022




in Section 4.

## 2 Data

In this study, we use the meteor radar observation to investigate the nonlinear interactions between the tides and atmospheric oscillations in the MLT. The meteor radar is situated at Wuhan (30.5°N, 114.6°E) in China, established by the Institute of Geology and Geophysics, Chinese Academy of Sciences (IGGCAS). This system is an all-sky interferometric meteor radar (Hocking et al., 2001), operating at 38.5 MHz. Meteor trails are illuminated by a three-element Yagi antenna directed toward the zenith with a transmitted peak power of 7.5 kW and a pulse repetition frequency of 1.98 kHz (Xiong et al., 2004; Jiang et al., 2005; Yu et al., 2013). Echoes reflected by meteor trails are detected by five three-element Yagi antennas oriented along two orthogonal baselines. The receiving antennas are sampled every 13.3 μs, resulting in a height resolution of 2 km. The hourly horizontal wind profile in the range of 70 to 110 km is deduced from the meteor trail velocities observed by radar, with a typical measurement uncertainty of 2-4 $ms^{-1}$ around 88-90 km (Hocking et al., 2001). The zonal and meridional winds for 9 years from 1 January 2012 to 31 December 2020 are applied to this investigation.

The number of meteor counts detected by radar showed a strong dependence on height, with an approximately Gaussian distribution centered at about 88-90 km, thus the data availability is high around 88-90 km. As the height goes up and down, the number of detected meteors decreases, and then the acceptable data reduces gradually. In the period of our concern, including several gaps with the maximum missing data of 53 days, the data availability exceeds 80% in the height range of 80-96 km, and then decreases to 69% at 98 km and 67% at 78 km, but is less than 50% above 98 km and below 78 km. In this case, the radar observation in the altitude range of 78-98 km is chosen for our study.

Considering that the zonal wavenumber of planetary scale perturbations cannot be deduced from the

https://doi.org/10.5194/acp-2022-407
Preprint. Discussion started: 15 August 2022


Atmospheric Chemistry and Physics Discussions

observations at a single station, we derive the zonal wavenumber from a two-dimensional Fourier transform with the help of Modern-Era Retrospective analysis for Research and Applications version 2 (MERRA2) reanalysis data. The upper pressure level at 0.01 hPa in the MERRA2 corresponds to the altitudes of about 78-80 km, which are largely consistent with the lower limit of the radar observation utilized. The MERRA2 data is produced by the Goddard Earth Sciences Data and Information Services Center (GES DISC) of the National Aeronautics and Space Administration (NASA) with some updates relative to the previous version (Gelaro et al., 2017), accessible from the online website at https://gmao.gsfc.nasa.gov/reanalysis/MERRA-2/. The reanalysis data is 6-hourly instantaneous analysis fields on a 0.5° × 0.625° latitude-by-longitude grid at 72 pressure levels from the ground up to 0.01 hPa level (Gelaro et al. 2017). The reanalysis zonal and meridional winds for a same period from 1 January 2012 to 31 December 2020 are used in this study.

## 3. Results

### 3.1 Resonant Interactions between DT/SDT and AO/SAO

Figure 1 shows the daily mean zonal and meridional winds from 78 to 98 km observed by the meteor radar at Wuhan for 9 years from 1 January 2012 to 31 December 2020. The different scale perturbations can be seen in the zonal and meridional wind fields.

Lomb-Scargle spectrum analysis is appropriate for decomposing unevenly sampled data into perturbation components (Scargle, 1982). In order to obtain the dominant periods in the wind fields, a Lomb-Scargle spectrum analysis, with a 4-times oversampling, is carried out on the zonal and meridional winds from the meteor radar observation between 1 January 2012 and 31 December 2020. Figures 2a and 2b present the Lomb-Scargle spectra of the zonal and meridional winds at 90 km, respectively. One can intuitively see from Figures 2a and 2b that the DT, SDT and low frequency oscillations are the prominent components, and the terdiurnal tide is also obvious. At Wuhan, the DT has the spectral amplitude of 17.7

https://doi.org/10.5194/acp-2022-407
Preprint. Discussion started: 15 August 2022




and 16.9 $ms^{-1}$ in the zonal and meridional winds, which are stronger than those of 9.6 and 12.1 $ms^{-1}$ for the SDT, respectively. The terdiurnal tide has the magnitude of about 2.2 $ms^{-1}$ in both the zonal and meridional winds.

For the sake of clarity, we zoom in on the several dominant spectral components. Figures 2c and 2d depict the low-frequency part (period >50 days) of the Lomb-Scargle spectra of the zonal and meridional winds, respectively, and then the strong AO and SAO can be clearly identified from the low-frequency components. In the zonal wind, the amplitude (12.3 $ms^{-1}$) of the AO is more intense than that (6.2 $ms^{-1}$) of the SAO, while in the meridional wind, the magnitude (4.6 $ms^{-1}$) of the SAO is larger than that (3.5 $ms^{-1}$) of the AO. Besides the AO, SAO and tides mentioned above, only the 16-day planetary wave (not presented) in the zonal wind has the spectral magnitude of about 2.1 $ms^{-1}$, and all the other spectral amplitudes in the zonal and meridional winds are smaller than 2 $ms^{-1}$. Hence, from the perspective of 9-year mean results, the diurnal and semidiurnal tides and annual and semiannual oscillations are the predominant perturbations in the MLT at 30.5°N.

Figures 2e and 2f show the spectra centered at the DT in the zonal and meridional winds, respectively. It is interesting that the DT spectra in Figures 2a and 2b are divided into multiple spectrum peaks in the zoomed-in Figures 2e and 2f. We note that these spectral peaks around the DT are right at the sum and difference frequencies between the DT and the annual and semiannual oscillations. Since the unexpected components satisfy the sum and different resonant conditions of $\omega_1 \pm \omega_2 = \omega_3$ with the DT and the AO/SAO, they should be excited through the nonlinear resonant interactions between the DT and the AO/SAO. In the zonal wind, the secondary waves excited by the tidal difference (sum) resonant interactions with the AO and SAO have the magnitudes of 10.6 and 6.8 $ms^{-1}$ (6.5 and 8.4 $ms^{-1}$), respectively. In the meridional wind, the excited waves in the difference (sum) resonant interactions between the DT and the AO and SAO have the intensities of 16.9 and 8.6 $ms^{-1}$ (9.9 and 8.5 $ms^{-1}$), respectively. Hence, these excited waves are much stronger than the terdiurnal tide with the amplitude of 2.2 ms$^{-1}$ in both the zonal and meridional winds. Moreover, it is surprising that in the tidal difference resonant interaction with the AO, the spectral amplitude (16.9 ms$^{-1}$) of the secondary wave in the meridional wind is larger than that (14.4 ms$^{-1}$) of the DT. Therefore, the spectral peak at the DT in Figure 2b is actually the peak of the generated secondary wave rather than the DT. Similarly, Figures 2g and 2h illustrate the occurrence of the resonant interactions between the SDT and the AO and SAO.

Now that the wavenumber matching conditions of $n_1 \pm n_2 = n_3$ should be satisfied in the resonant interactions, we examine the zonal wavenumber relation with the aid of the MERRA2 reanalysis data. The reanalysis zonal and meridional winds at 0.01 hPa (~ 80 km) at 30.5°N for the same period of 9 years are selected to make a two-dimensional Fourier transform. Figure 3 shows the zoomed-in frequency-wavenumber spectra around the AO and SAO and the DT. In Figure 3, we use the sign $\delta$ to denote the frequency of the AO (1/365 day$^{-1}$), and the negative wavenumber represents the westward propagation of wave. One can clearly see from Figure 3 that the zonal wavenumbers in both the zonal and meridional winds are 0 for the AO and SAO and -1 for the DT, as we all know. The spectral peaks on both sides of the DT are located not only at the sum and difference frequencies between the DT and the AO/SAO, similar to the results of the radar observation in Figure 2, but also just at the wavenumber of -1, indicating that the wavenumber matching conditions of $n_1 \pm n_2 = n_3$ are satisfied. Hence, this confirms that these new components are generated through the nonlinear resonant interactions between the DT and the AO/SAO. In addition, the similar phenomenon arises in the zoomed-in frequency-wavenumber spectra around the SDT with the zonal wavenumber of -2 (not presented), too.

### 3.2 Spectral Amplitude Variation with Altitude

Here, we investigate the magnitude variation of these generated waves with height. From the Lomb-Scargle spectra of the zonal and meridional winds for the period of 9 years observed by the meteor radar, we extract the spectral amplitudes of the DT/SDT, AO/SAO, and secondary waves at altitude range of 78-98 km. Figure 4 shows the amplitude evolution of the four components in the interactions of the DT with the AO (upper panels) and the SAO (lower panels). In the zonal wind, the amplitude of the AO decreases sharply from 21.7 $ms^{-1}$ at 78 km to only 1.9 $ms^{-1}$ at 86 km, and then increases rapidly to 17.0 $ms^{-1}$ at 98 km, while the SAO diminishes gradually from 14.1 $ms^{-1}$ at 78 km to 3.6 $ms^{-1}$ at 98 km. In the meridional wind, the AO tends to reduce with height, but the opposite is true for the SAO. As for the DT, its vertical variations roughly resemble each other in the zonal and meridional winds, with the peak magnitudes of about 21.0 and 16.9 $ms^{-1}$ at 94 km, respectively. Interestingly, in the difference resonant interaction between the DT and the AO, the generated wave has the maximum amplitudes of 12.5 and 18.5 $ms^{-1}$ in the zonal and meridional winds at 94 km, and its vertical evolution is similar to that of the DT. In particular, in the meridional wind above 86 km, the secondary wave is more intense than the DT. In the sum resonant interaction, the secondary wave in the meridional wind increases to the maximum amplitude of 10.8 $ms^{-1}$ at 88 km, and then decreases monotonously with altitude, while in the zonal wind, after experiencing a decline from 88 km to 92 km, its amplitude grows up with height again. Whereas, in the sum and difference resonant interactions between the DT and SAO, the excited waves show the trend of first increasing and then decreasing with height, and have the maximum magnitudes at the heights slightly lower than 94 km.

Figure 5 depicts the variation of the four components in the interactions of the SDT with the AO (upper panels) and the SAO (lower panels). The SDT is strengthened in the zonal wind with the rising height, but is attenuated in the meridional wind after reaching the peak at 90 km. The amplitudes of these secondary waves vary with altitude. The secondary wave generated through the sum resonant interaction of the SDT with the AO is stronger in the meridional wind at 94-98 km than the SDT. On the whole, except at a few heights, the magnitudes of the SDT and SAO in the MLT at Wuhan are smaller than those of the DT and AO, respectively, thus the secondary waves in the interactions between the SDT and SAO are generally weaker

https://doi.org/10.5194/acp-2022-407
Preprint. Discussion started: 15 August 2022

Atmospheric Chemistry and Physics Discussions
Open Access
EGU

than those in the interactions between the DT and AO. In addition, since the work due to Reynolds stress in a sheared flow can lead to significant energy exchanges between wave and flow (Huang et al, 2010) and the wave dissipation from molecular and eddy diffusions is closely related to the wave scale (Huang et al., 2014), the magnitudes of the generated waves may also be associated with their dissipation and coupling with the background flow after they are excited.

## 4. Summary

In this paper, we use the meteor radar observations and MERRA2 reanalysis data of 9 years to demonstrate the occurrence of the resonant interactions between the DT/SDT and the AO/SAO in the MLT.

The Lomb-Scargle spectra of the zonal and meridional winds at 90 km show that only the AO, SAO, DT and SDT are the predominant components in both the zonal and meridional winds with the spectral amplitudes of 3.5-17.7 $ms^{-1}$. The terdiurnal tide is a relatively strong component with the magnitude of 2.2 $ms^{-1}$ in the zonal and meridional winds, and the 16-day PW has the amplitude of 2.1 $ms^{-1}$ in the zonal wind. Except these, all the other spectral amplitudes are smaller than 2 $ms^{-1}$.

When we zoom in on the partial spectra centered the DT, there exist several significant peaks in the upper and lower sidebands of the DT. These spectral peaks are located right at the sum and difference frequencies between the DT and the AO and SAO, meaning that these waves are generated through the nonlinear resonant interactions between the DT and the AO/SAO. The amplitudes of the secondary waves excited through the difference (sum) resonant interactions between the DT and the AO and SAO attain the large values of 10.6 and 6.8 $ms^{-1}$ (6.5 and 8.4 $ms^{-1}$) in the zonal wind, and 16.9 and 8.6 $ms^{-1}$ (9.9 and 8.5 $ms^{-1}$) in the meridional winds, respectively, which are far stronger than the amplitude (2.2 $ms^{-1}$) of the terdiurnal tide. In particular, the secondary wave in the difference resonant interaction between the DT and the AO has the larger amplitude (16.9 $ms^{-1}$) in the meridional wind than the DT (14.4 $ms^{-1}$). The frequency-wavenumber

https://doi.org/10.5194/acp-2022-407
Preprint. Discussion started: 15 August 2022




spectra of the reanalysis zonal and meridional winds at 0.01 hPa (~80 km) indicate that the zonal wavenumber of the DT, AO and secondary waves is -1, 0 and -1, respectively, confirming that the resonant conditions of wavenumbers in the interactions are met. Similarly, the matching conditions of wavenumbers and frequencies are also satisfied for the triads of the SDT, AO/SAO and secondary waves. Therefore, the nonlinear resonant interactions between the DT/SDT and the AO/SAO do occur in the MLT.

In the height range of 78-98 km, the secondary waves in the interactions between the SDT and SAO are weaker than those in the interactions between the DT and AO because the amplitude of the SDT and SAO are generally smaller than those of the DT and AO, respectively. At some altitudes, the secondary waves have the larger amplitude than the DT/SDT, thus in the tidal studies, the magnitude of the secondary waves may be treated as the intensity of the tides when the time series of data is not long enough or the spectral components are not distinguished carefully.

**Data availability.** The meteor radar observations are provided by the IGGCAS and the Chinese Meridian Project at the website of http://wdc.geophys.ac.cn/, and the MERRA2 reanalysis data is from the NASA GES DISC at https://gmao.gsfc.nasa.gov/reanalysis/MERRA-2/ (Gelaro et al., 2017).

**Author contributions**. KH proposed the scientific ideas. XH and KH completed the analysis and the manuscript. HC, SZ, CH, and YG discussed the results in the manuscript.

**Competing interests.** The contact author has declared that neither they nor their co-authors have any competing interests.

**Acknowledgments.** We thank the IGGCAS and the Chinese Meridian Project for providing the meteor radar data, and the NASA for providing the MERRA2 reanalysis data.

**Financial support.** This research has been supported by the National Natural Science Foundation of China (grant nos. 41974176, 42174189 and 42127805).

## References

Achatz, U., Ribstein, B., Senf, F., and Klein, R.: The interaction between synoptic-scale balanced flow and a finite-amplitude mesoscale wave field throughout all atmospheric layers: weak and moderately strong stratification, Q. J. Roy. Meteor. Soc., 143, 342-361, https://doi.org/10.1002/qj.2926, 2017.

Andrews, D. G., Holton, J. R., and Leovy, C. B.: Middle atmosphere dynamics, 1st edn., vol. 40, edited by: Dmowska, R., and Holton, J. R., San Diego, Calif., Academic Press Inc, p. 489, ISBN: 9780120585762, 1987.

Axelsson, P., Larsson, J., and Stenflo, L.: Nonlinear interaction between acoustic gravity waves in a rotating atmosphere, Nonlinear Proc. Geoph., 3, 216-220, https://doi.org/10.5194/npg-3-216-1996, 1996.

Babu, V. S., Kumar, K. K., John, S. R., Subrahmanyam, K. V., and Ramkumar, G.: Meteor radar observations of short-term variability of quasi 2 day waves and their interaction with tides and planetary waves in the mesosphere-lower thermosphere region over Thumba (8.5°N, 77°E), J. Geophys. Res., 116, D16121, https://doi.org/10.1029/2010JD015390, 2011.

Chang, L. C., Liu, J.-Y., and Palo, S. E.: Propagating planetary wave coupling in SABER MLT temperatures and GPS TEC during the 2005/2006 austral summer, J. Geophys. Res., 116, A10324, https://doi.org/10.1029/2011JA016687, 2011a.

Chang, L. C., Palo, S. E., and Liu, H.-L.: Short-term variability in the migrating diurnal tide caused by interactions with the quasi 2 day wave, J. Geophys. Res., 116, D12112, https://doi.org/10.1029/2010JD014996, 2011b.

Chapman, S. and Lindzen, R. S.: Atmospheric tides, 1st edn., Springer Dordrecht, Dordrecht, Holland, https://doi.org/10.1007/978-94-010-3399-2, 1970.

https://doi.org/10.5194/acp-2022-407
Preprint. Discussion started: 15 August 2022



Chatterjee, D. and Misra, A. P.: Effects of Coriolis force on the nonlinear interactions of acoustic-gravity waves in the atmosphere, J. Atmos. Sol.-Terr. Phy., 222, 105722, https://doi.org/10.1016/j.jastp.2021.105722, 2021.

Cheng, H., Huang, K. M., Liu, A. Z., Zhang, S. D., Huang, C. M., and Gong, Y.: A quasi-27-day oscillation activity from the troposphere to the mesosphere and lower thermosphere at low latitudes, Earth Planets Space, 73, 183, https://doi.org/10.1186/s40623-021-01521-1, 2021.

Eckermann, S. D., Rajopadhyaya, D. K., and Vincent, R. A.: Intraseasonal wind variability in the equatorial mesosphere and lower thermosphere: Long-term observations from central Pacific, J. Atmos. Sol.-Terr. Phy., 59, 603-627, https://doi.org/10.1016/S1364-6826(96)00143-5, 1997.

Fritts, D. C., Sun, S. J., and Wang, D. Y.: Wave-wave interactions in compressible atmosphere: 1. A general formulation including rotation and wind shear, J. Geophys. Res., 97, 9975-9988, https://doi.org/10.1029/92JD00347, 1992.

Forbes, J. M. and Garrett, H. B.: Theoretical studies of atmospheric tides, Rev. Geophys., 17, 1951-1981, https://doi.org/10.1029/RG017i008p01951, 1979.

Gelaro, R., McCarty, W., Suárez, M. J., Todling, R., Molod, A., Takacs, L., Randles, C. A., Darmenov, A., Bosilovich, M. G., Reichle, R., Wargan, K., Coy, L., Cullather, R., Draper, C., Akella, S., Buchard, V., Conaty, A., da Silva, A. M., Gu, W., Kim, G.-K., Koster, R., Lucchesi, R., Merkova, D., Nielsen, J. E., Partyka, G., Pawson, S., Putman, W., Rienecker, M., Schubert, S. D., Sienkiewicz, M., and Zhao, B.: The modern-era retrospective analysis for research and applications, version 2 (MERRA-2), J. Climate, 30, 5419-5454, https://doi.org/10.1175/JCLI-D-16-0758.1, 2017.

Hagan, M. E., Burrage, M. D., Forbes, J. M., Hackney, J., Randel, W. J., and Zhang, X.: GSWM-98: results for migrating solar tides, J. Geophys. Res., 104, 6813-6827, https://doi.org/10.1029/1998JA900125, 1999.

He, M. and Chau, J. L.: Mesospheric semidiurnal tides and near-12 h waves through jointly analyzing observations of five specular meteor radars from three longitudinal sectors at boreal midlatitudes, Atmos. Chem. Phys., 19, 5993-6006, https://doi.org/10.5194/acp-19-5993-2019, 2019.

Hocking, W. K., Fuller, B., and Vandepeer, B.: Real-time determination of meteor-related parameters

https://doi.org/10.5194/acp-2022-407
Preprint. Discussion started: 15 August 2022

Atmospheric Chemistry and Physics
Discussions

utilizing modern digital technology, J. Atmos. Sol.-Terr. Phy., 63, 155-169, https://doi.org/10.1016/S1364-6826(00)00138-3, 2001.

Huang, K. M., Zhang, S. D., and Yi, F.: Gravity wave excitation through resonant interaction in a compressible atmosphere, Geophys. Res. Lett., 36, L01803, https://doi.org/10.1029/2008GL035575, 2009.

Huang, K. M., Zhang, S. D., and Yi, F.: Reflection and transmission of atmospheric gravity waves in a stably sheared horizontal wind field, J. Geophys. Res., 115, D16103, https://doi.org/10.1029/2009JD012687, 2010.

Huang, K. M., Liu, A. Z., Lu, X., Li, Z., Gan, Q., Gong, Y., Huang, C. M., Yi, F., and Zhang, S. D.: Nonlinear coupling between quasi 2 day wave and tides based on meteor radar observations at Maui, J. Geophys. Res.-Atmos., 118, 10936-10943, https://doi.org/10.1002/jgrd.50872, 2013a.

Huang, K. M., Liu, A. Z., Zhang, S. D., Yi, F., Huang, C. M., Gan, Q., Gong, Y., and Zhang, Y. H.: A nonlinear interaction event between a 16-day wave and a diurnal tide from meteor radar observations, Ann. Geophys., 31, 2039-2048, https://doi.org/10.5194/angeo-31-2039-2013, 2013b.

Huang, K. M., Zhang, S. D., Yi, F., Huang, C. M., Gan, Q., Gong, Y., and Zhang, Y. H.: Nonlinear interaction of gravity waves in a nonisothermal and dissipative atmosphere, Ann. Geophys., 32, 263-275, https://doi.org/10.5194/angeo-32-263-2014, 2014.

Inhester, B.: Numerical modeling of hydromagnetic wave coupling in the magnetosphere, J. Geophys. Res.-Space, 92, 4751-4756, https://doi.org/10.1029/JA092iA05p04751, 1987.

Jacobi, Ch., Schminder, R., and Kürschner, D.: Non-linear interaction of the quasi 2-day wave and long-term oscillations in the summer midlatitude mesopause region as seen from LF D1 wind measurements over Central Europe (Collm, 52°N, 15°E), J. Atmos. Sol.-Terr. Phy., 60, 1175-1191, https://doi.org/10.1016/S1364-6826(98)00076-5, 1998.

Jacobi, Ch., Portnyagin, Yu. I., Merzlyakov, E. G., Kashcheyev, B. L., Oleynikov, A. N., Kürschner, D., Mitchell, N. J., Middleton, H. R., Muller, H. G., and Comley, V. E.: Mesosphere/lower thermosphere wind measurements over Europe in summer 1998, J. Atmos. Sol.-Terr. Phy., 63, 1017-1031, https://doi.org/10.1016/S1364-6826(01)00012-8, 2001.

Jacobi, Ch., Fröhlich, K., and Pogoreltsev, A.: Quasi two-day-wave modulation of gravity wave flux and

https://doi.org/10.5194/acp-2022-407
Preprint. Discussion started: 15 August 2022




consequences for the planetary wave propagation in a simple circulation model, J. Atmos. Sol.-Terr. Phy., 68, 283-292, https://doi.org/10.1016/j.jastp.2005.01.017, 2006.

Jiang, G., Xiong, J.-G., Wan, W.-X., Ning, B.-Q., Liu, L.-B., Vincent, R. A., and Reid, I.: The 16-day waves in the mesosphere and lower thermosphere over Wuhan (30.6°N, 114.5°E) and Adelaide (35°S, 138°E), Adv. Space Res., 35, 2005-2010, https://doi.org/10.1016/j.asr.2005.03.011, 2005.

Kamalabadi, F., Forbes, J. M., Makarov, N. M., and Portnyagin, Yu. I.: Evidence for nonlinear coupling of planetary waves and tides in the Antarctic mesopause, J. Geophys. Res., 102, 4437-4446, https://doi.org/10.1029/96JD01996, 1997.

Klostermeyer, J.: Two- and three-dimensional parametric instabilities in finite-amplitude internal gravity waves, Geophys. Astro. Fluid, 61, 1-25, https://doi.org/10.1080/03091929108229035, 1991.

Kumar, K. K., Deepa, V., Antonita, T. M., and Ramkumar, G.: Meteor radar observations of short-term tidal variabilities in the low-latitude mesosphere-lower thermosphere: Evidence for nonlinear wave-wave interactions, J. Geophys. Res., 113, D16108, https://doi.org/10.1029/2007JD009610, 2008.

Lindzen, R. S. and Chapman, S.: Atmospheric tides, Space Sci. Rev., 10, 3-188, https://doi.org/10.1007/BF00171584, 1969.

Liu, H.-L., Li, T., She, C.-Y., Oberheide, J., Wu, Q., Hagan, M. E., Xu, J., Roble, R. G., Mlynczak, M. G., and Russell III, J. M.: Comparative study of short-term diurnal tidal variability, J. Geophys. Res., 112, D18108, https://doi.org/10.1029/2007JD008542, 2007.

McCormack, J. P., Eckermann, S. D., Hoppel, K. W., and Vincent, R. A.: Amplification of the quasi-two day wave through nonlinear interaction with the migrating diurnal tide, Geophys. Res. Lett., 37, L16810, https://doi.org/10.1029/2010GL043906, 2010.

Müller, P., Holloway, G., Henyey, F., and Pomphrey, N.: Nonlinear interactions among internal gravity waves, Rev. Geophys., 24, 493-536, https://doi.org/10.1029/RG024i003p00493, 1986.

Palo, S. E., Forbes, J. M., Zhang, X., Russell III, J. M., and Mlynczak, M. G.: An eastward propagating two-day wave: Evidence for nonlinear planetary wave and tidal coupling in the mesosphere and lower thermosphere, Geophys. Res. Lett., 34, L07807, https://doi.org/10.1029/2006GL027728, 2007.

Pancheva, D. V. and Mitchell, N. J.: Planetary waves and variability of the semidiurnal tide in the mesosphere and lower thermosphere over Esrange (68°N, 21°E) during winter, J. Geophys. Res., 109, A08307, https://doi.org/10.1029/2004JA010433, 2004.

Pancheva, D. V., Beard, A. G., and Mitchell, N. J.: Nonlinear interactions between planetary waves in the mesosphere/lower-thermosphere region, J. Geophys. Res., 105, 157-170, https://doi.org/10.1029/1999JA900332, 2000.

Pancheva, D., Merzlyakov, E., Mitchell, N. J., Portnyagin, Y., Manson, A. H., Jacobi, Ch., Meek, C. E., Luo, Y., Clark, R. R., Hocking, W. K., MacDougall, J., Muller, H. G., Kürschner, D., Jones, G. O. L., Vincent, R. A., Reid, I. M., Singer, W., Igarashi, K., Fraser, G. I., Fahrutdinova, A. N., Stepanov, A. M., Poole, L. M. G., Mailga, S. B., Kashcheyev, B. L., and Oleynikov, A. N.: Global-scale tidal variability during the PSMOS campaign of June-August 1999: Interaction with planetary waves, J. Atmos. Sol.-Terr. Phy., 64, 1865-1896, https://doi.org/10.1016/S1364-6826(02)00199-2, 2002.

Phillips, O. M.: On the dynamics of unsteady gravity waves of finite amplitude Part 1. The elementary interactions, J. Fluid Mech., 9, 193-217, https://doi.org/10.1017/S0022112060001043, 1960.

Scargle, J. D.: Studies in astronomical time series analysis: II. Statistical aspects of spectral analysis of unevenly spaced data, Astrophys. J., 263, 835-853, https://doi.org/10.1086/160554, 1982.

Stenflo, L.: Resonant three-wave interactions in plasmas, Phys. Scripta, T50, 15-19, https://doi.org/10.1088/0031-8949/1994/T50/002, 1994.

Stenflo, L.: Nonlinear equations for acoustic gravity waves, Phys. Scripta, T75, 306, http://dx.doi.org/10.1238/physica.topical.075a00306, 1998.

Stenflo, L. and Shukla, P. K.: Nonlinear acoustic-gravity waves, J. Plasma Phys., 75, 841-847, https://doi.org/10.1017/S0022377809007892, 2009.

Taklo, T. M. A. and Choi, W.: Group resonant interactions between surface and internal gravity waves in a two-layer system, J. Fluid Mech., 892, A14, https://doi.org/10.1017/jfm.2020.180, 2020.

Teitelbaum, H., and Vial, F.: On tidal variability induced by nonlinear interaction with planetary waves, J. Geophys. Res., 96, 14169-14178, https://doi.org/10.1029/91JA01019, 1991.

Vanneste, J.: The instability of internal gravity waves to localized disturbances, Ann. Geophys., 13, 196–210, https://doi.org/10.1007/s00585-995-0196-7, 1995.

Voelker, G. S., Akylas, T. R., and Achatz, U.: An application of WKBJ theory for triad interactions of internal gravity waves in varying background flows, Q. J. Roy. Meteor. Soc., 147, 1112-1134,

https://doi.org/10.5194/acp-2022-407
Preprint. Discussion started: 15 August 2022


Atmospheric Chemistry and Physics Discussions

https://doi.org/10.1002/qj.3962, 2021.

Wüst, S. and Bittner, M.: Non-linear resonant wave-wave interaction (triad): Case studies based on rocket data and first application to satellite data, J. Atmos. Sol.-Terr. Phy., 68, 959-976, https://doi.org/10.1016/j.jastp.2005.11.011, 2006.

Xiong, J.-G., Wan, W., Ning, B., and Liu, L.: First results of the tidal structure in the MLT revealed by Wuhan meteor radar (30°40′N, 114°30′E), J. Atmos. Sol.-Terr. Phy., 66, 675-682, https://doi.org/10.1016/j.jastp.2004.01.018, 2004.

Yeh, K. C., and Liu, C. H.: The instability of atmospheric gravity waves through wave-wave interactions, J. Geophys. Res., 86, 9722-9728, https://doi.org/10.1029/JC086iC10p09722, 1981.

Yi, F.: Resonant interactions between propagating gravity wave packets, J. Atmos. Sol.-Terr. Phy., 61, 675-691, https://doi.org/10.1016/S1364-6826(99)00026-7, 1999.

Yu, Y., Wan, W., Ning, B., Liu, L., Wang, Z., Hu, L., and Ren, Z.: Tidal wind mapping from observations of a meteor radar chain in December 2011, J. Geophys. Res., 118, 2321-2332, https://doi.org/10.1029/2012JA017976, 2013.

Yue, J., Liu, H.-L., and Chang, L. C.: Numerical investigation of the quasi 2 day wave in the mesosphere and lower thermosphere, J. Geophys. Res., 117, D05111, https://doi.org/10.1029/2011JD016574, 2012.

https://doi.org/10.5194/acp-2022-407
Preprint. Discussion started: 15 August 2022


Atmospheric Chemistry and Physics Discussions

**Caption:**

**Figure 1.** Daily mean (a) zonal and (b) meridional winds at 78-98 km between 1 January 2012 and 31 December 2020 from meteor radar observation at Wuhan.

**Figure 2.** Lomb-Scargle spectra of (a) zonal and (b) meridional winds at 90 km from radar observation of 9 years and their zoomed-in views around frequencies corresponding to (c, d) AO and SAO, (e, f) DT and (g, h) SDT. The left and right columns denote the spectra of the zonal and meridional winds, respectively. The red (blue) dashed vertical line is marked at the frequency of the AO (SAO) in Panels (c, d), and the sum and difference frequencies between the DT and the AO (SAO) in Panels (e, f) and between the SDT and the AO (SAO) in Panels (g, h).

**Figure 3.** Zoomed-in views of frequency-wavenumber spectra of zonal and meridional winds at 0.01 hPa at 30.5°N around frequencies corresponding to (a, b) AO and SAO and (c, d) DT derived from MERRA2 reanalysis data of 9 years. The sign $\delta$ is the frequency of AO (1/365 day$^{-1}$), and the left and right columns denote the spectra of the zonal and meridional winds, respectively. The negative wavenumber represents the westward phase progression. The dotted horizontal lines are marked at the frequencies of the AO and SAO in Panels (a, b), and at the frequency of the DT and the sum and difference frequencies between the DT and the AO/SAO in Panels (c, d). The dotted vertical lines are marked at the wavenumber of 0 in Panels (a, b) and -1 in Panels (c, d).

**Figure 4.** Spectral amplitudes of (blue) DT, (red) AO, (yellow) SAO, and (purple solid) sum and (purple dashed) difference frequency secondary waves generated through resonant interactions between DT and AO/SAO in (left) zonal and (right) meridional winds at 78-90 km. Panels (a, b) show the amplitudes of the DT, AO and secondary waves, and Panels (c, d) show the amplitudes of the DT, SAO and secondary waves.

**Figure 5.** Spectral amplitudes of (green) SDT, (red) AO, (yellow) SAO, and (purple solid) sum and (purple dashed) difference frequency secondary waves generated through resonant interactions between SDT and

https://doi.org/10.5194/acp-2022-407
Preprint. Discussion started: 15 August 2022


Atmospheric Chemistry and Physics Discussions

AO/SAO in (left) zonal and (right) meridional winds at 78-90 km. Panels (a, b) show the amplitudes of the SDT, AO and secondary waves, and Panels (c, d) show the amplitudes of the SDT, SAO and secondary waves.

https://doi.org/10.5194/acp-2022-407
Preprint. Discussion started: 15 August 2022

Atmospheric Chemistry and Physics Discussions

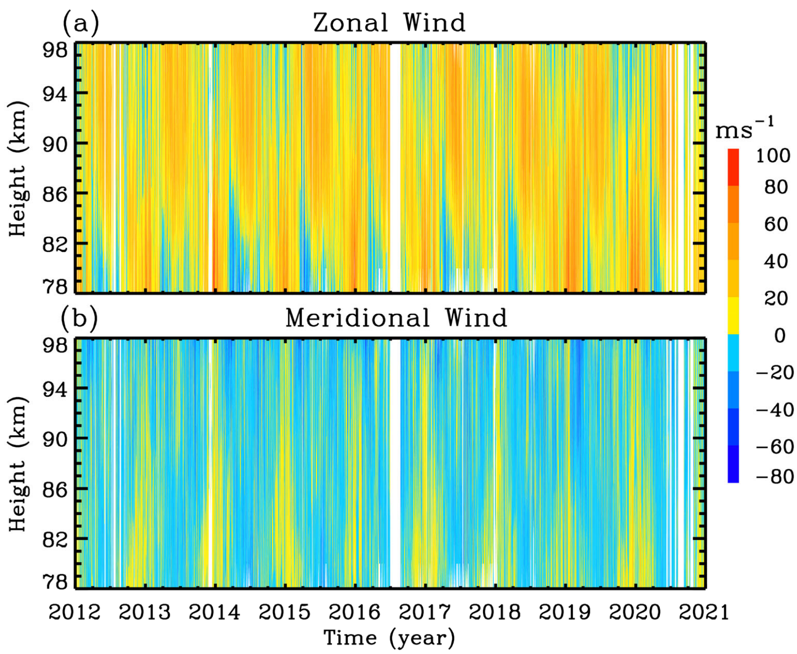


**Figure 1.** Daily mean (a) zonal and (b) meridional winds at 78-98 km between 1 January 2012 and 31 December 2020 from meteor radar observation at Wuhan.

https://doi.org/10.5194/acp-2022-407
Preprint. Discussion started: 15 August 2022


Atmospheric Chemistry and Physics
Discussions

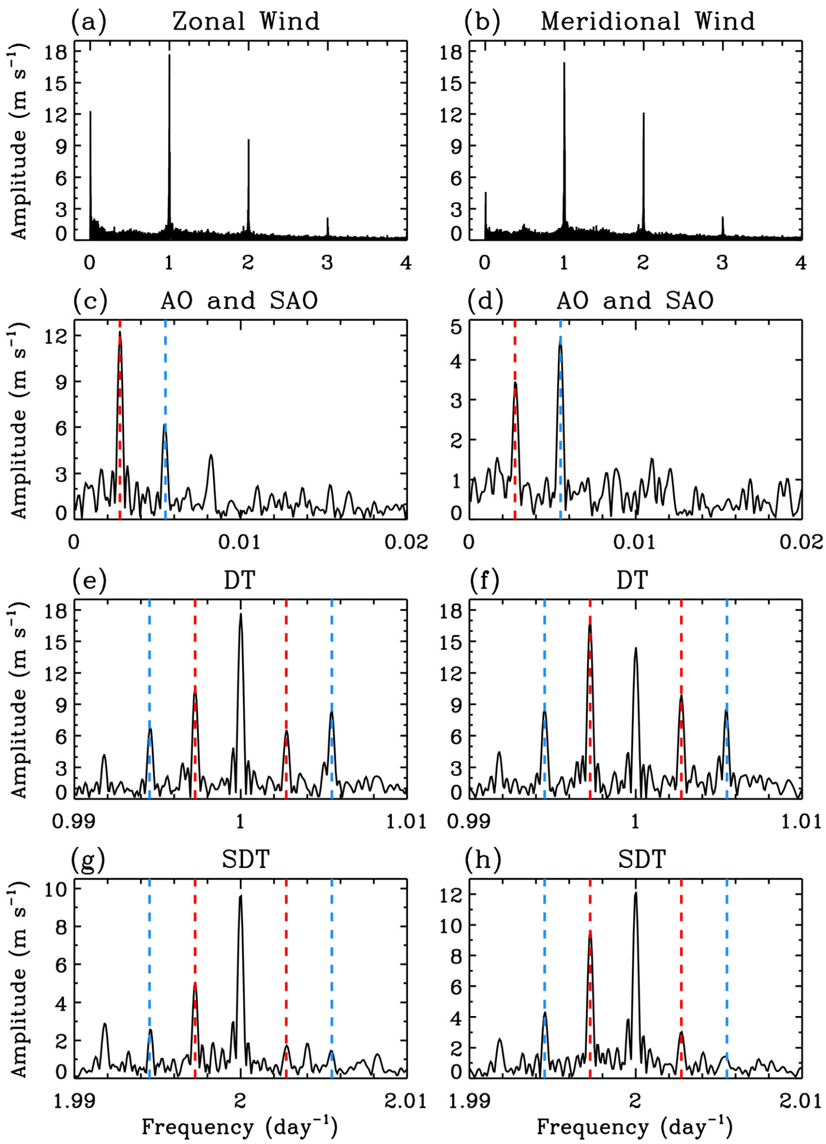


**Figure 2.** Lomb-Scargle spectra of (a) zonal and (b) meridional winds at 90 km from radar observation of 9 years and their zoomed-in views around frequencies corresponding to (c, d) AO and SAO, (e, f) DT and (g, h) SDT. The left and right columns denote the spectra of the zonal and meridional winds, respectively. The red (blue) dashed vertical line is marked at the frequency of the AO (SAO) in Panels (c, d), and the sum and difference frequencies between the DT and the AO (SAO) in Panels (e, f) and between the SDT and the AO (SAO) in Panels (g, h).

https://doi.org/10.5194/acp-2022-407
Preprint. Discussion started: 15 August 2022



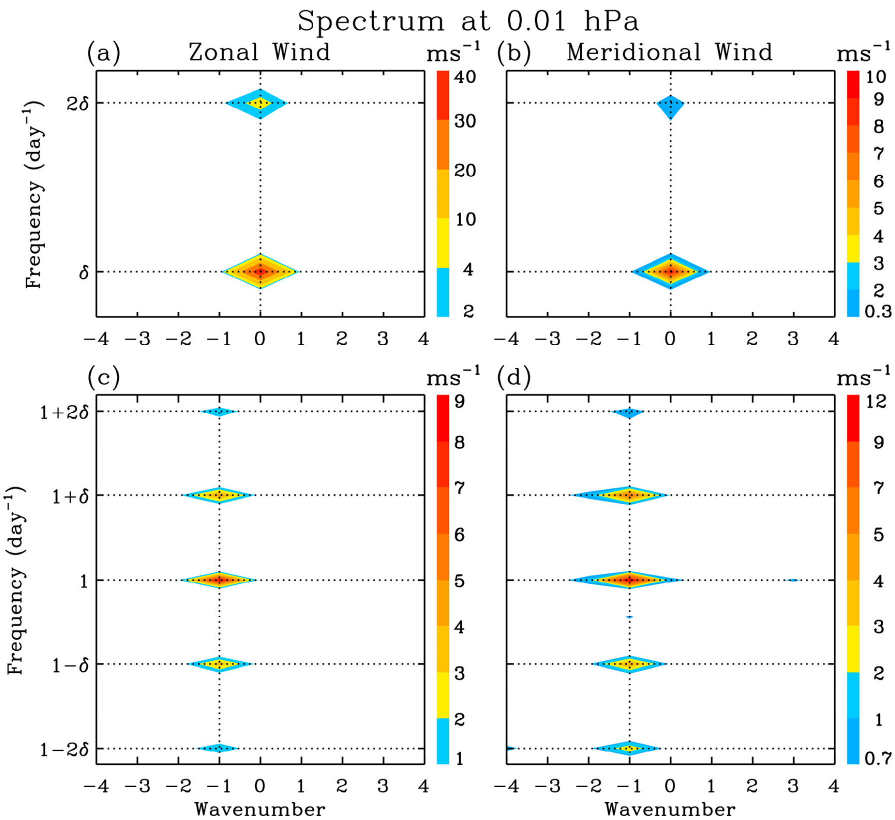


**Figure 3.** Zoomed-in views of frequency-wavenumber spectra of zonal and meridional winds at 0.01 hPa at 30.5°N around frequencies corresponding to (a, b) AO and SAO and (c, d) DT derived from MERRA2 reanalysis data of 9 years. The sign $\delta$ is the frequency of AO (1/365 day$^{-1}$), and the left and right columns denote the spectra of the zonal and meridional winds, respectively. The negative wavenumber represents the westward phase progression. The dotted horizontal lines are marked at the frequencies of the AO and SAO in Panels (a, b), and at the frequency of the DT and the sum and difference frequencies between the DT and the AO/SAO in Panels (c, d). The dotted vertical lines are marked at the wavenumber of 0 in Panels (a, b) and -1 in Panels (c, d).

https://doi.org/10.5194/acp-2022-407
Preprint. Discussion started: 15 August 2022


Atmospheric Chemistry and Physics
Open Access
Discussions

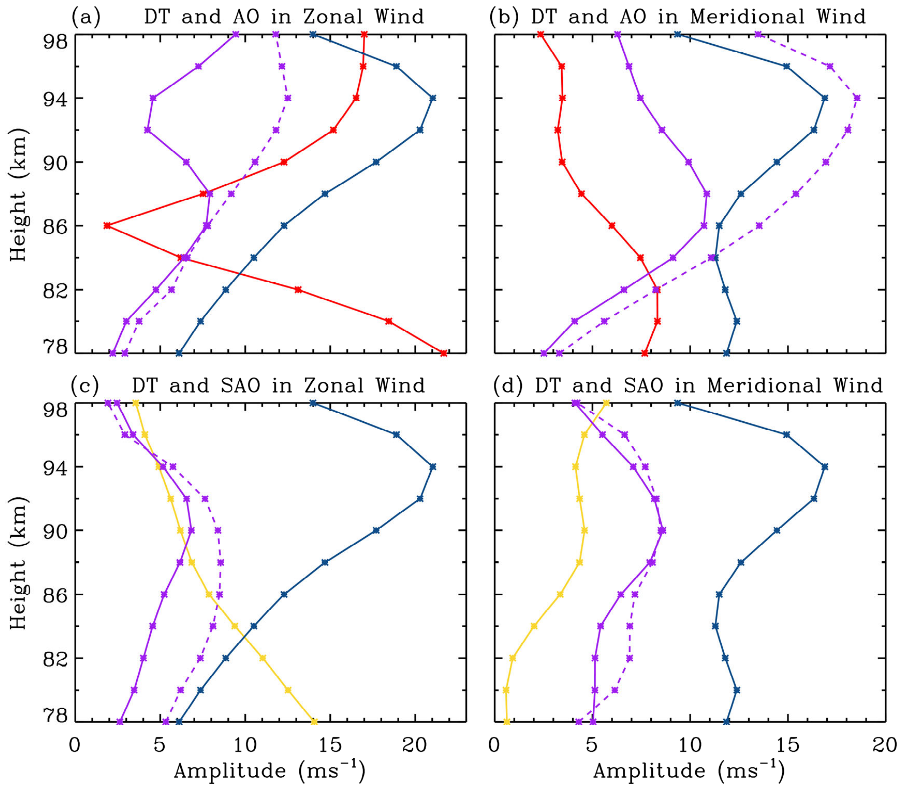


**Figure 4.** Spectral amplitudes of (blue) DT, (red) AO, (yellow) SAO, and (purple solid) sum and (purple dashed) difference frequency secondary waves generated through resonant interactions between DT and AO/SAO in (left) zonal and (right) meridional winds at 78-90 km. Panels (a, b) show the amplitudes of the DT, AO and secondary waves, and Panels (c, d) show the amplitudes of the DT, SAO and secondary waves.

https://doi.org/10.5194/acp-2022-407
Preprint. Discussion started: 15 August 2022


Atmospheric Chemistry and Physics
Discussions

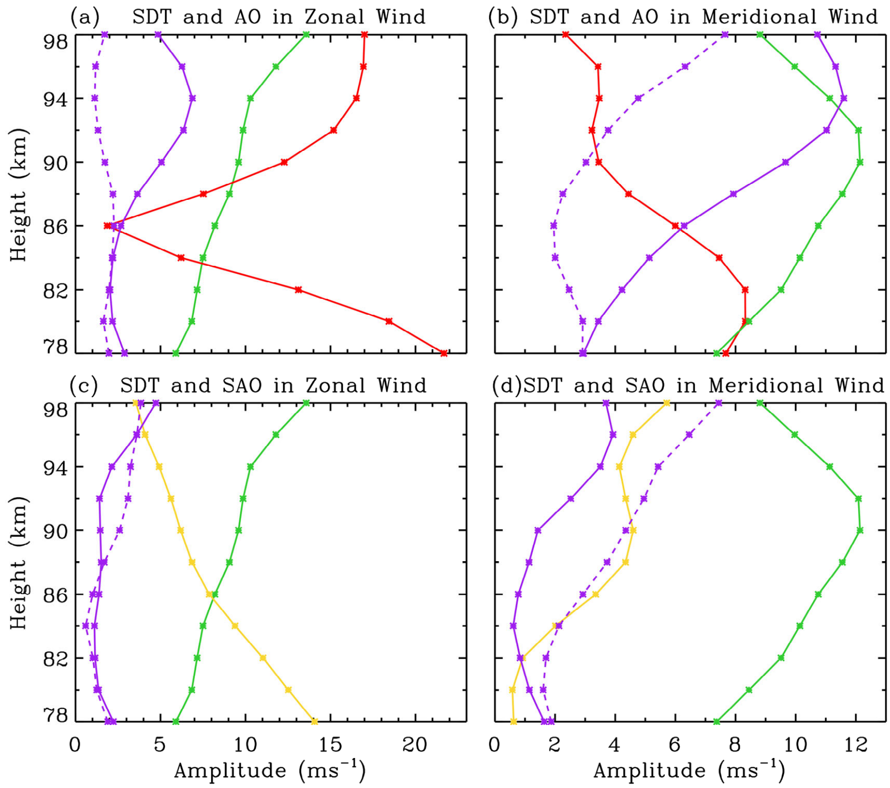


**Figure 5.** Spectral amplitudes of (green) SDT, (red) AO, (yellow) SAO, and (purple solid) sum and (purple dashed) difference frequency secondary waves generated through resonant interactions between SDT and AO/SAO in (left) zonal and (right) meridional winds at 78-90 km. Panels (a, b) show the amplitudes of the SDT, AO and secondary waves, and Panels (c, d) show the amplitudes of the SDT, SAO and secondary waves.